Icarus 349 (2020) 113870

Contents lists available at ScienceDirect

Icarus

journal homepage: www.elsevier.com/locate/icarus

The ionosphere of Venus: Strongest control by photo-chemical-equilibrium in the solar system, with implications for exospheric temperatures

M. Mendillo [a], J. Trovato [a], C. Narvaez [a,*], P. Withers [a], M. Pätzold [b], K. Peter [b], S. Tellmann [b], B. Häusler [c]

[a] Center for Space Physics, Boston University, Boston, MA 02215, United States of America
[b] Rheinisches Institut für Umweltforschung an der Universität zu Köln, Abteilung Planetenforschung, Cologne, Germany
[c] Institut für Raumfahrttechnik und Weltraumnutzung, Universität der Bundeswehr München, Neubiberg, Germany

ARTICLE INFO

Keywords:
Venus ionosphere
Radio occultation data
Photo-chemical models
Venus exospheric temperature

ABSTRACT

Profiles of electron density versus height obtained by the radio occultation experiment on Venus Express provide an observational data base suitable for semi-empirical modeling. The basic equations of photo-chemical-equilibrium (PCE) theory can be applied to the altitude range 100–170 km of Venus' ionosphere (Peter et al., 2014). Within that domain, the maximum electron density (N_{max}) and total electron content (TEC) show very high correlations (0.98) with parameterizations of solar flux and solar zenith angle. Validation using independent profiles from the Venera 15/16 radio occultation experiments yielded an even higher correlation (0.99). Such dominance of PCE ionospheric processes at Venus is the highest in the solar system. This allows for N_{max} and TEC to be used to derive estimates of the exospheric temperature of Venus' thermosphere at ~170 km.

1. Introduction

The first observation of the ionosphere at Venus was made using the radio occultation technique on 19 October 1967 during the Mariner V mission (Kliore et al., 1967). The ionospheric profile exhibited a layer of maximum electron density of ~5.5 × 10^5 e^-/cm^3 at ~140 km, with a secondary layer of 2 × 10^5 e^-/cm^3 at ~125 km. This fundamental signature of Venus' plasma environment was published two years after the first documentation of Mars' ionosphere by Mariner IV (Kliore et al., 1965). The field of comparative ionospheres was thus created for the three terrestrial planets known to have permanent atmospheres.

There are many excellent reviews of the neutral and plasma components of the upper atmosphere at Venus. The most recent comprehensive account is by Gérard et al. (2017) and references therein. Ionospheric patterns and processes for the primary and secondary layers are discussed in even greater detail by Peter et al. (2014). Girazian et al. (2015) presented a comprehensive summary of the low altitude secondary layer produced by X-rays.

For both Venus and Mars, it is customary to offer parameterizations of ionospheric parameters as a function of solar flux and solar zenith angle (see, for example, Fox and Yeager (2009) for Mars).

For Venus, Kliore and Mullen (1989) provided a parameterization of maximum electron density (N_{max}) versus the 10.7 cm radio proxy for solar flux (F_{sun}) of the form

$$N_{max}(F_{sun}) = Constant(\#1) \times (F_{sun})^{\alpha} \quad (1)$$

An additional parameterization was used for solar zenith angle (SZA),

$$N_{max}(SZA) = Constant(\#2) \times [cos(SZA)]^{\beta} \quad (2)$$

where Constant (#2) = N_{max}(SZA = 0°)

Finally, merged parameterizations used both parameters,

$$N_{max}(F_{sun}, SZA) = Constant(\#3) \times (F_{sun})^{\alpha} \times [cos(SZA)]^{\beta} \quad (3)$$

Much attention has been given to the values of the exponents α and β. For the Kliore and Mullen (1989) study, α = 0.376 ± 0.011 and β = 0.511 ± 0.012. As discussed in detail by Fox and Yeager (2006, 2009), and summarized below, for an ionosphere governed by photo-chemical-equilibrium (PCE), electron densities are proportional to the square root of both solar flux and solar zenith angle, and thus α = β = 0.5 is required (as adopted by Chapman, 1931a, 1931b). There are several reasons why observations and their analyses might not yield the 0.5 exponent, and none suggest that PCE physics is in error (Fox and Yeager, 2006). For

* Corresponding author.
E-mail address: cnarvaez@bu.edu (C. Narvaez).

https://doi.org/10.1016/j.icarus.2020.113870
Received 18 December 2019; Received in revised form 27 April 2020; Accepted 22 May 2020
Available online 30 May 2020

example, an ionospheric data set might have calibration uncertainties, the solar radio flux measured at Earth is far from a perfect proxy for EUV and X-ray irradiance at a planet, and non-PCE processes such as neutral and plasma dynamics add complexities to otherwise pure PCE drivers. For the solar irradiance issue at Mars, Girazian and Withers (2013) demonstrated that when the solar EUV and soft X-ray observations are made at Mars, the PCE exponent 0.5 emerges as the correct one to use. Thus, our approach will be to adopt PCE as the appropriate formalism, thus fixing the exponent at 0.5, and determine the resulting correlations in their most general form using

$$N_{max} = C_1 \times [F_{sun} \times cos(SZA)]^{1/2} + C_2 \quad (4)$$

where the operational value of F_{sun} is defined below. Our goal is to arrive at parameterizations of maximum electron density and N_e(h) integrated total electron content of the Venus ionosphere using the formal equations of PCE collectively represented by Eq. (4). We will derive our semi-empirical model results using an under-utilized set of radio occultation observations from the Mars Express radio science experiment, with validations coming from observations made during prior missions. The results will provide a versatile parameterization/prediction scheme similar to that available from the Mars Initial Reference Ionosphere (MIRI) most recently described in Mendillo et al. (2018a).

2. Semi-empirical modeling

We will adopt for nomenclature in all that follows the practice of identifying ionospheric layers numerically from lower altitude (#1) to upper altitude (#2), together with a letter to identify the planet (Rishbeth and Mendillo, 2004; Mendillo, 2019). Thus, for Venus the secondary layer produced by the sun's soft X-rays is the V1-layer, typically at 125 km, with its maximum electron density designated N_mV_1. The primary layer produced by solar EUV is the V2 layer with maximum electron density near 140 km designated as N_mV_2 (Pätzold et al., 2007). For Earth, these are called the *E*- and F1-layers (Bauer and Lammer, 2004), with the same terminology often used for Mars (Fox and Yeager, 2009).

Our approach to semi-empirical modeling of Venus' ionosphere is similar to that used to formulate the Mars Initial Reference Ionosphere (MIRI) model described in Mendillo et al. (2013, 2018a). The goal is to specify values of the maximum electron density at Venus (N_mV_2) and the integral of the electron density profile, defined as the total electron content (TEC), as a function of coupled solar flux and solar zenith angle (SZA) for daytime conditions (SZA < 90°). Previous studies (e.g., Peter et al., 2014) have shown that at the height of maximum electron density, the Venus ionosphere is governed by photo-chemical-equilibrium (PCE)—the balance of production and loss (Rishbeth and Garriott, 1969; Fox and Yeager, 2006; Schunk and Nagy, 2009). Under such conditions, production by solar ionizing radiation ($P \sim F_{sun}$) is balanced by the quadratic loss term for electron density ($L \sim N_e^2$) and thus $N_e \sim [F_{sun}]^{1/2}$. Away from the sub-solar point, $F_{sun} \rightarrow F_{sun}$ (SZA = 0°) × cos (*SZA*), as shown in equation (329) in Rishbeth and Garriott (1969). Since F_{sun} varies with distance (d in AU) from the Sun as $1/d^2$, $N_e \sim 1/d$, This is a general pattern that holds for PCE ionospheric layers throughout the solar system (see Figure 1 in Mendillo et al., 2003).

All other processes and parameters involved in PCE conditions that contribute to variability of peak electron density are considered to be secondary. These include changes in the composition of the neutral atmosphere, effects of electron temperature on plasma recombination rates, uncertainties about ionization cross sections, secondary ionization rates, and chemical reaction rates—plus all forms of dynamics (neutral and plasma). The fact that success can be achieved using this remarkably simple approach is testimony of how dominant PCE conditions can be in a plasma composed of molecular ions and electrons in a very dense neutral atmosphere.

To quantify the solar ionization driver of a PCE ionosphere, one needs to deal with the value of solar flux at the sub-solar point and its variation with latitude and local time—collectively described by solar zenith angle (SZA). Given that measurements of solar irradiance values (X-ray and EUV photon flux vs. wavelength) are not available at Venus, the long-standing practice is to characterize solar output by the Sun's radio flux at 10.7 cm (F10.7) observed on a daily basis at Earth. To relate these proxy solar fluxes measured at Earth to ionospheric observations made at Venus, the positions of both planets in their elliptical orbits must be taken into account. The protocol adopted is to transform all observations to an equivalent circular orbit for Venus (0.723 AU), and use the PCE equations at that fixed distance from the Sun to formulate the model.

We now use N_mV_2 values to describe the approach. For TEC, an identical scheme is followed, but with integrations to different topside altitudes to show pure-PCE versus PCE-plus-dynamics effects. For each day of an observation at Venus, the following steps are carried out:

a. Determine the date when the side of the Sun facing Venus was observed at Earth in order to select the appropriate daily value of F10.7 to use. This is called "the rotated Sun date" – a correction that can span ±14 days (being zero when Venus is at inferior conjunction, i.e., on the Sun - Venus - Earth line).
b. Convert the observed flux at Earth to its equivalent value at d = 0.723 AU using the $1/d^2$ correction for sunlight, where the $1/(0.723)^2$ factor increases the flux by 1.91.
c. Transform the rotated-sun-date F10.7 value at 0.723 AU to an effective solar flux (F_{eff}) obtained by smoothing the daily value with a three solar rotation (81-day) average (Schunk and Nagy, 2009):

$$F_{eff} = \frac{F10.7_{(day)} + \langle F10.7 \rangle_{(81-day)}}{2} \text{ [all at d = 0.723 AU]} \quad (5)$$

Convert the values of N_mV_2 observed at distance d(AU) to their representative values at d = 0.723 AU using the PCE equation $N_e \sim 1/d$.

$$N_mV_2(0.723AU) = N_mV_2(d) \times d(AU)/0.723 \quad (6)$$

d. Use the values F_{eff} and N_mV_2 at d = 0.723 AU and cos(SZA) in the PCE equation

$$N_mV_2 \sim \sqrt{F_{eff} \times cos(SZA)} \quad (7a)$$

$$\text{defining a PCE factor as } F_{PCE} = \sqrt{F_{eff} \times cos(SZA)} \quad (7b)$$

to determine the functional form of the correlation arising from simple PCE processes. See Rishbeth and Garriott (1969) and Mendillo et al., 2018a for derivation of Eqs. (7a) and (7b). We do not use the grazing incidence formula (Smith and Smith, 1972) in place of cos(SZA) because it requires prior knowledge of the scale height of the neutral atmosphere (Rishbeth and Garriott, 1969). Testing with a neutral scale height of 5 km at h_{max} = 140 km, the error introduced by not using the Chapman function is <10% for SZA < 86 °.

Using a data set of N_mV_2, F_{eff} and SZA yields the best-fit linear correlation,

$$N_mV_2 = C_1\sqrt{F_{eff} \times cos(SZA)} + C_2 \quad (8)$$

This equation is suitable for all daytime conditions given by SZA = 0° to 90°. Moreover, it provides a "default" value of N_mV_2 beyond the solar terminator (sunset and dawn). That is, $N_mV_2 = C_2$, when the cosine term (with SZA = 90°) eliminates the first term in the equation.

e. Finally, while our study of PCE behavior is conducted at the fixed distance of 0.723 AU, the value derived from Eq. (8) can be adjusted to a different orbital distance from the Sun by using Eq. (6).

3. Data sources and analysis

Our goal of using photo-chemical-equilibrium (PCE) physics as the

basis for semi-empirical modeling requires "daytime" data sets (SZA < 90°) with altitude coverage for electron density $N_e(h)$ from below the V1-layer to the topside ionosphere (~ 250 km) in order to identify the maximum electron density (N_mV_2) and to have comprehensive profiles to integrate for TEC. This eliminates using the vast amount of in-situ observations by Pioneer Venus Orbiter (PVO) because the PVO orbit did not have a periapse low enough to define unambiguously the value of N_mV_2 (see figure 3 in Colin, 1979). The PVO radio occultation experiments did provide full $N_e(h)$ profiles (numbering 94) that are available from the National Space Science Data Center (NSSDC). Yet, the vast majority were for near-terminator or nighttime conditions (SZA > 80°), and thus unsuitable for our goal. Additional PVO radio occultation data (30 profiles) for SZA = 30° – 170° in the NSSDC are in poorly archived graphical formats, also unsuitable for our goals. Yet, 14 values of only the peak electron density (N_mV_2) are given in Table 2 of Ambili et al. (2019), and we will use these for additional model validations.

Far more promising are two Venus ionosphere data sets from radio occultation experiments conducted during the Venera 15 & 16 missions (Gavrik et al., 2010) and the Venus Express (VEX) mission (Häusler et al., 2006; Pätzold et al., 2007; Gérard et al., 2017). The Venera data pertain to SZA = 55° – 90° (29 profiles) and the VEX Radio Occultation (VeRa) data span SZA = 5° – 90° (217 profiles). We will use the more abundant VeRa data to derive our Venus PCE model and the Venera observations as test/validation data.

Fig. 1 shows the 217 VeRa electron density profiles sorted by SZA values. This is a somewhat larger data base than the 174 VeRa profiles used in Girazian et al. (2015) to study the V1-layer (their Fig. 2). As can be seen, the values of N_mV_2 are easily identified, and SZA coverage is excellent. The VeRa observations span the period 14 July 2006 to 16 January 2014, thus offering excellent solar cycle coverage.

The altitude range 100–250 km spans the ionospheric domains of pure photo-chemical-equilibrium (PCE) conditions to PCE-plus-dynamics. While the transition does not occur abruptly at some specific height, the two regions can be separated at the altitude where the time constants for chemistry are equal to the time constant for plasma dynamics. A very similar case occurs at Mars within the same altitude domain. In Figure 16 of Mendillo et al. (2011), these altitudes were computed to be ~150 km for O_2^+ and ~ 180 km for O^+. Peter et al. (2014) adopted a single height of 170 km. For Venus, we will use that value in this paper. It appears as a dashed line in Fig. 1.

Further characterization of this data set is presented in Fig. 2. In the top panel, the SZAs offer a rare occurrence of broad coverage for a radio occultation experiment (9° – 85°). The second panel describes solar flux conditions measured at 1 AU (with equivalent values at Venus (0.723 AU) being ~1.9 stronger). The N_mV_2 values, adjusted to 0.723 AU, appear in the third panel and exhibit a broad distribution. The fourth panel shows minimal changes in the height of maximum electron density (h_{max}) with an average of 140.7 ± 2 km (Gérard et al., 2017). This panel is for context only since values of h_{max} are not used in our parameterizations (Eqs. (11) and (12)). Total electron content (TEC) values (integrated vertically between 100 and 250 km), again at 0.723 AU, appear in the bottom panel and exhibit a distribution consistent with expectations from the N_mV_2 pattern. The VeRa observations thus provide an excellent data source for semi-empirical modeling.

The application of Eq. (4) to the VeRa N_mV_2 observations results in Fig. 3. The linear correlation coefficient of 0.98 confirms the visual conclusion of a remarkably well ordered peak electron density in the ionosphere at Venus.

4. Validation

The 29 $N_e(h)$ profiles from the Venera 15/16 data set in the Planetary Data System (PDS) are relatively small in number, but have the asset of being all daytime observations and thus well suited for testing a daytime ionospheric model. Using the same format as in Fig. 1, we show the $N_e(h)$ profiles in Fig. 4, with a statistical summary in Fig. 5 (using the same format as in Fig. 2). Panel 5(a) shows that the Venera SZAs occur in the 55° to 90° range—narrower than for VeRa, but still a good sample of conditions. The solar flux pattern in panel (b) shows a somewhat narrower cluster of medium solar cycle values than shown in Fig. 2. In panel (c), the N_mV_2 values span a factor of three, while their h_{max} values are tightly clustered between 135 and 150 km (panel d) with the average

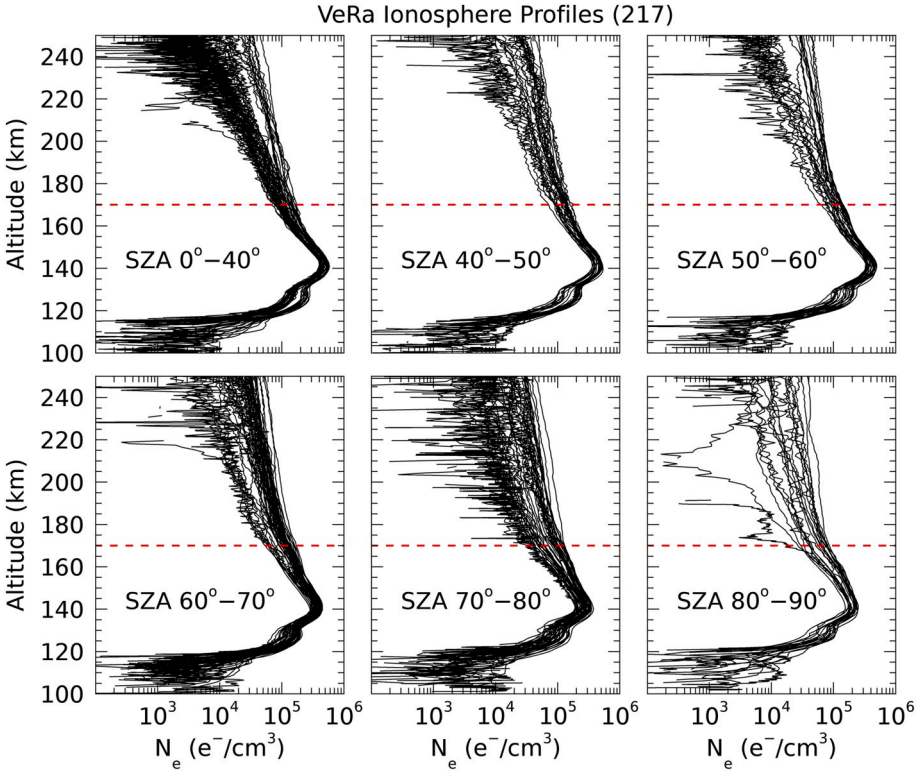

Fig. 1. Set of 217 electron density profiles from the VeRa radio occultation experiment on Venus Express. The $N_e(h)$ data span heights from 100 km to 250 km, sub-divided using six solar zenith angle bins. In the analyses that follow, three parameters are used: The value of maximum electron density (N_mV_2), the height of maximum density (h_{max}), and the integrated profiles for total electron content (TEC). Note that all data are for "daytime" conditions, i.e., with solar zenith angles <90°. The dashed red line at 170 km indicates the altitude where pure PCE conditions transition to PCE + dynamics. (For interpretation of the references to color in this figure legend, the reader is referred to the web version of this article.)

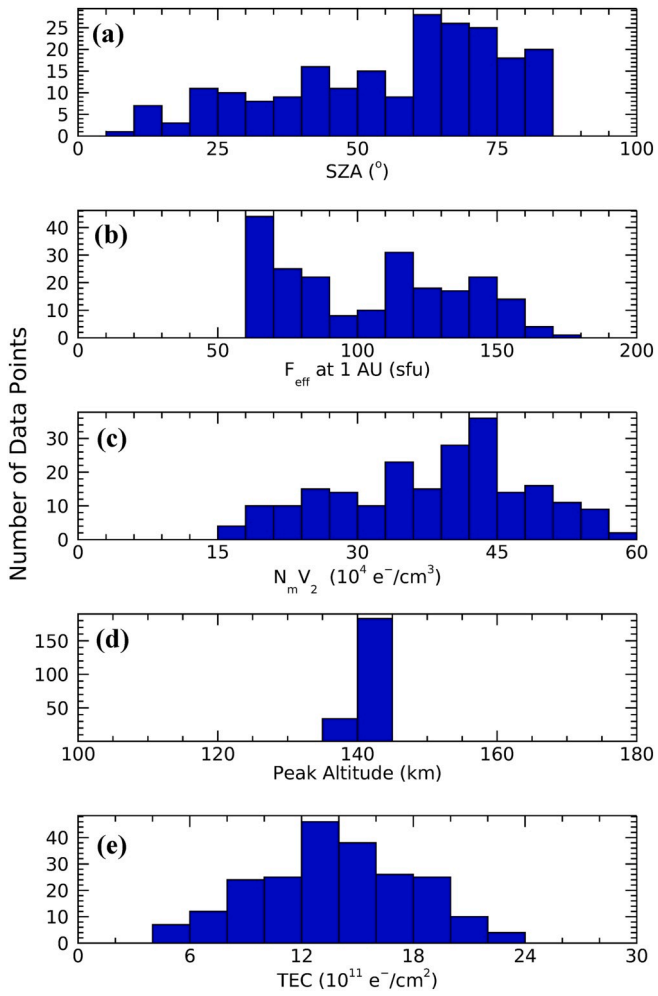

Fig. 2. Statistical summary of the data shown in Fig. 1. Panel (a) gives the solar zenith angle distribution, (b) the effective solar fluxes [see text and Eq. (5)], (c) values of maximum electron density (N_mV_2) at 0.723 AU, (d) heights of maximum electron density, and (e) total electron content values at 0.723 AU in TEC units (TECU) defined as $10^{11} e^-/cm^2$ (recall that at Earth 1 TECU = 10^{16} e^-/m^2).

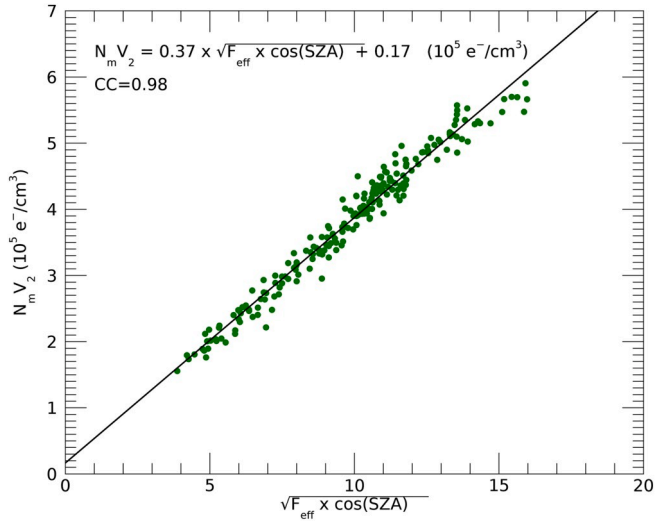

Fig. 3. Distribution of the 217 N_mV_2 values shown in Fig. 1 versus the photochemical-equilibrium factor (F_{PCE}) defined in Eqs. (7a) and (7b). The resultant equation and its correlation coefficient (CC) are indicated.

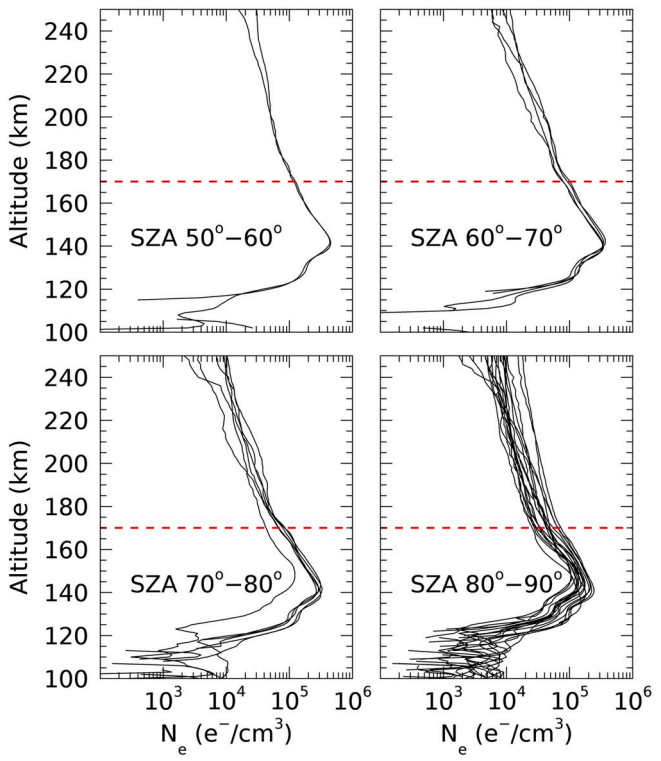

Fig. 4. Set of 29 electron density profiles from the Venera 15/16 radio occultation experiment. The $N_e(h)$ data span heights from 100 km to 250 km, subdivided using four solar zenith angle bins. Note that all data are for "daytime" conditions, i.e., with solar zenith angles <90°. The dashed red line at 170 km indicates the altitude where pure PCE conditions transition to PCE + dynamics (Peter et al., 2014). (For interpretation of the references to color in this figure legend, the reader is referred to the web version of this article.)

being ~140 km (Gérard et al., 2017). Finally, panel (e) shows that the TEC values span a factor of three, consistent with panel (c).

Using this data set and Eq. (4) yields the results shown in Fig. 6. The best-fit line is

$$N_mV_2 = (0.37 \pm 0.006) \times \sqrt{F_{eff} \times cos(SZA)} + (0.20 \pm 0.043)\ [\text{in units of } 10^5\ e^-/cm^3] \quad (9)$$

Its correlation coefficient of 0.996 is indistinguishable from that derived from the VeRa data in Fig. 3. Notice also that the PCE factor values on the horizontal axis extend the line in Fig. 3 to even lower values (due mainly to the higher SZA values).

As a second validation exercise, Table 2 of Ambili et al. (2019), extracted from Table 1 in Cravens et al. (1981), gives 14 values of peak electron density (N_mV_2) from the radio occultation experiment on Pioneer Venus Orbiter (PVO). While statistically small in number, these observations provide a valuable test during a period of very high solar activity (9 November 1979–22 September 1980) with F_{eff} at 1 AU 170–270 units. Using the same formats as in Figs. 2 and 5, our summary of the PVO data appears in Fig. 7, and the results of our PCE modeling are given in Fig. 8. The best fit equation (with a CC = 0.98) is

$$N_mV_2 = (0.396 \pm 0.024) \times \sqrt{F_{eff} \times cos(SZA)} - (0.127 \pm 0.348)\ [\text{in units of } 10^5\ e^-/cm^3] \quad (10)$$

We conclude that the representation of the maximum electron density in Venus' ionosphere is very well described by the equation in Fig. 3, namely,

$$N_mV_2 = (0.37 \pm 0.005) \times \sqrt{F_{eff} \times cos(SZA)} + (0.17 \pm 0.046)\ [\text{in units of } 10^5\ e^-/cm^3] \quad (11)$$

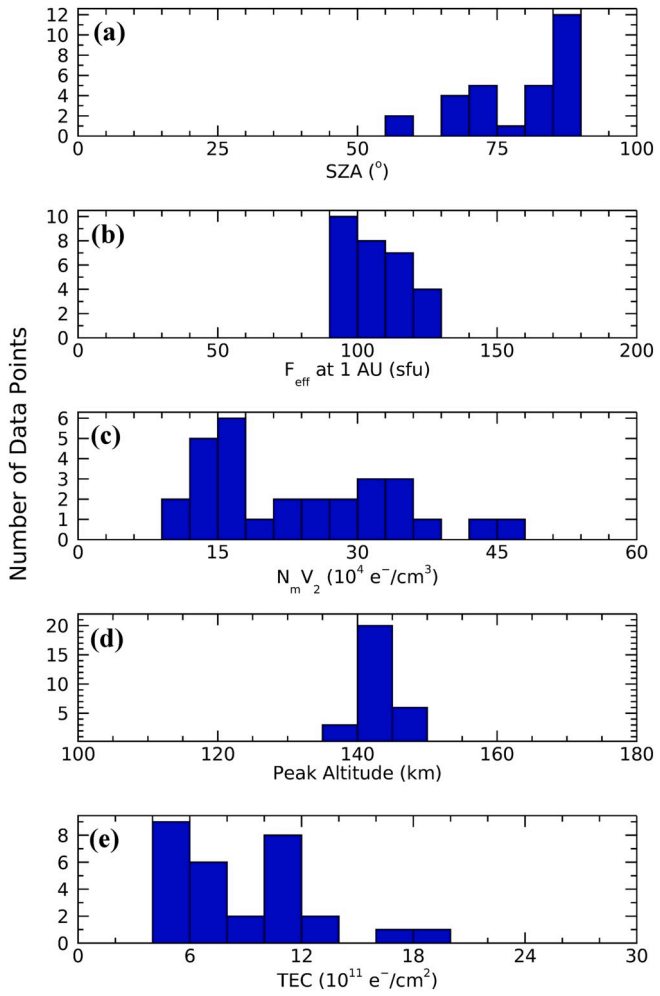

Fig. 5. Statistical summary of the 29 $N_e(h)$ profile parameters from the Venera 15/16 radio occultation experiments used to test the results in Fig. 3. Panel (a) gives the solar zenith angle distribution, (b) the effective solar fluxes, (c) values of maximum electron density at 0.723 AU, (d) heights of maximum electron density and (e) total electron content values at 0.723 AU.

While this equation is meant to represent the dayside ionosphere of Venus as determined by the two PCE parameters of solar flux and zenith angle, when SZA = 90° and the first term is zero, the constant provides a rough estimate of "post-sunset" conditions ($N_mV_2 \sim 17 \times 10^3$ e$^-$/cm^3). Zhang et al. (1990) showed examples of Venus peak electron densities after sunset (SZA = 103°-104°) to be in the range 18–27 $\times 10^3$ e$^-$/cm^3 for solar minimum and maximum conditions, respectively. For their SZA = 90°-100° bin, the range of peak densities was 10–40 $\times 10^3$ e$^-$/cm^3 over a full solar cycle. The value of the constant in Eq. (11) is a reasonable estimate of those values from semi-empirical modeling.

Peter et al. (2014) were the first to present a detailed analysis of the Venus Express radio occultation (VeRa) observations using 89 $N_e(h)$ profiles from the years 2006–2012. In their Fig. 13(a), there was a clear pattern of N_mV_2 versus SZA, with considerable scatter shown to be due to different solar flux conditions. In their Fig. 14(c), the same trend was shown for TEC values obtained from the same profiles. In our use of Eq. (8) with 217 VeRa $N_e(h)$ profiles providing N_mV_2 and TEC values, the combined dependences upon SZA and effective solar flux reduced the scatter to very low levels.

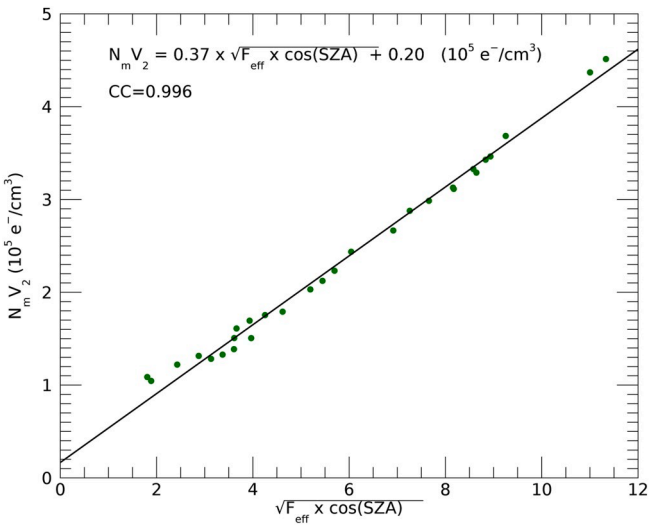

Fig. 6. Distribution of the 29 N_mV_2 values from Venera 15/16 (described in panel (c) of Fig. 5) versus the photo-chemical-equilibrium parameter defined in Eq. (8). For this "validation test" dataset the resultant equation and its correlation coefficient are indicated. Note the near identical results to those shown in Fig. 3.

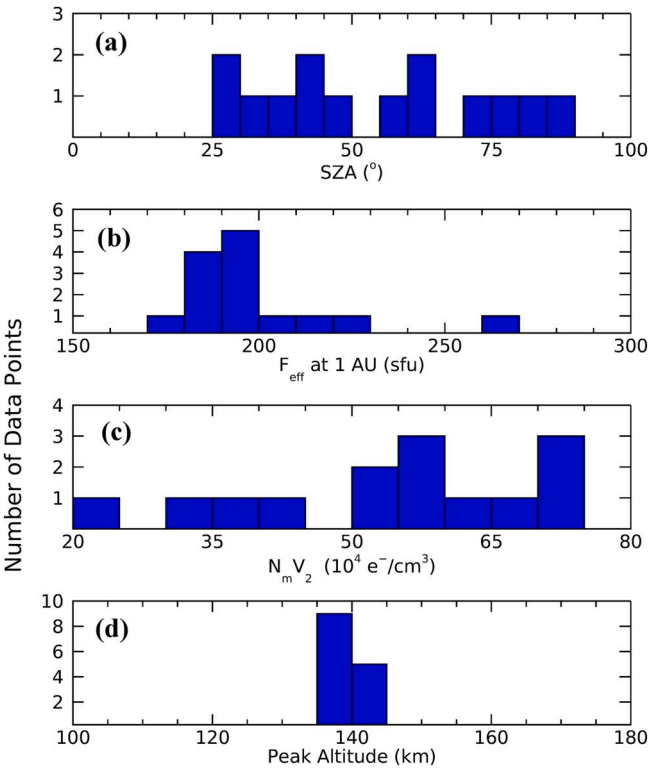

Fig. 7. Statistical summary of the 14 results from the radio occultation experiment on PVO, found in table 2 of Ambili et al., 2019, used to test the results in Fig. 3. Panel (a) gives the solar zenith angle distribution, (b) the effective solar fluxes, (c) values of maximum electron density at 0.723 AU, and (d) heights of maximum electron density.

5. Total electron content and equivalent slab thickness: implications for Venus' neutral atmosphere

5.1. Model for total electron content

Vertical integration of each of the $N_e(h)$ profiles shown in Fig. 1 (100

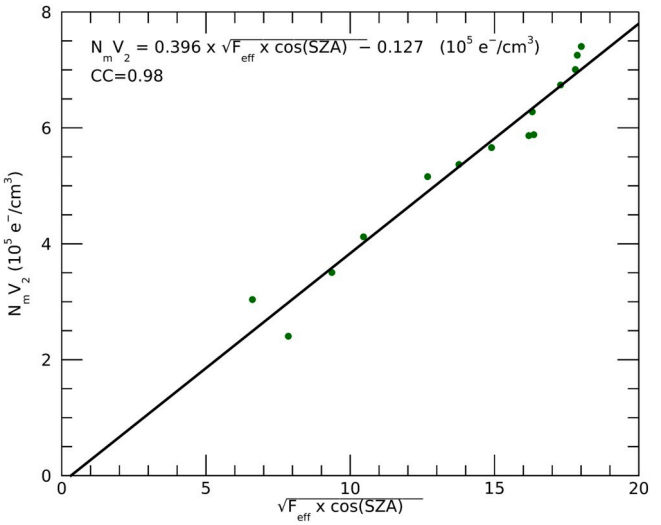

Fig. 8. Distribution of the 14 N_mV_2 values from PVO (described in panel (c) of Fig. 7) versus the photo-chemical-equilibrium parameter defined in Eq. (8). For this validation test dataset the resultant equation and its correlation coefficient are indicated.

to 250 km) yields the total electron content (TEC) of Venus' ionosphere. As shown in Fig. 2, the typical value for TEC of the Venus ionosphere is 12–14 TEC units (1 TECU = 1 × 10^{11} e^-/cm^2). Studies of TEC morphology at Mars using the MRO/SHARAD radar (Mendillo et al., 2017) yield an average daytime value of ~6–8 TECU. The factor of two larger TEC values at Venus vs Mars is consistent with PCE dominated ionospheres. As described above, peak electron density and thus TEC scale as 1/d from the Sun, and thus with Mars at 1.524 AU and Venus at 0.723 AU, their ratio is 2.1.

Using the same protocols developed for semi-empirical modeling of N_mV_2 data, applying Eq. (4) to TEC data yields the results shown in Fig. 9. The TEC equation corresponding to (5), with a correlation coefficient = 0.93, as shown in panel (a), is

$$\mathrm{TEC} = (1.43 \pm 0.039) \times \sqrt{\mathrm{F_{eff}} \times cos(\mathrm{SZA})} - (0.21 \pm 0.402)\ \left[\text{in units of } 10^{11}\ \mathrm{e^-/cm^2}\right] \quad (12)$$

While the constant C_2 from Eq. 8 is a very small numerical correction (−0.21) to the first term, one cannot have a negative TEC value when SZA = 90°. We thus consider Eq. (12) to be appropriate for daytime (SZA < 90°) conditions only.

In panel (b) of Fig. 9, the altitude limits for vertical TEC are reduced to the photo-chemical-equilibrium domain (100–170 km) as described in Peter et al. (2014). The variability is clearly less, resulting in the higher correlation coefficient of 0.98. Again, the C_2 constant is small and negative, with negligible impact on the numerical results.

5.2. Model for equivalent slab thickness

The ratio τ = TEC/N_mV_2 has the unit of length. It describes the breadth (in kilometers) of a slab of plasma with uniform electron density equal to N_mV_2 that, when integrated, matches the TEC. Since TEC and N_mV_2 are highly correlated, τ varies far less than either parameter and thus serves as a practical way to estimate one from the other (Fox et al., 1991). When both are known, the scientific use of τ arises from the finding that under PCE conditions, the resultant ionosphere is strongly dependent upon the distribution of neutral gases in the atmosphere. Based on the results shown in Figure 12 of Peter et al. (2014), PCE conditions hold up to the height where temperature becomes isothermal, approximately 170 km. Thus τ values are a first-order indicator of the scale height (H = kT/mg), and hence the temperature of the background neutral atmosphere at ~170 km. To evaluate H, k is

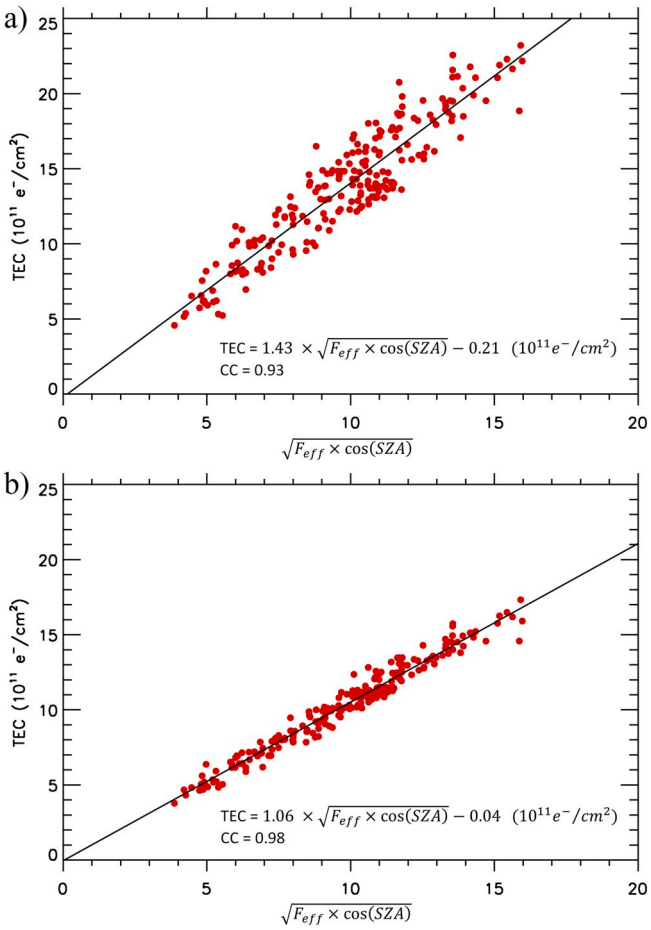

Fig. 9. Distribution of the 217 TEC values derived from integration of the $N_e(h)$ profiles in Fig. 1 versus the photo-chemical-equilibrium parameter defined in Eq. 8. In panel (a) the limits of integration are 100–250 km, while in panel (b) they are 100–170 km to show the differences between broad altitude limits versus the PCE-only domain. The resultant equations and correlation coefficients are indicated.

Boltzmann's constant, T is temperature in degrees Kelvin, m is mass of the dominant gas, and g is the acceleration due to gravity at the surface.

Wright (1960) showed that when a $N_e(h)$ profile follows the functional pattern associated with Chapman Theory, its integral results in TEC = 4.133 × H × N_{max}, where N_{max} is the maximum electron density and 4.133 is a numerical integration factor. Thus, for Venus

$$\tau = \frac{\mathrm{TEC}}{\mathrm{N_mV_2}} = 4.133\ \mathrm{x}\ H = 4.133 \times \mathrm{kT} \Big/ \mathrm{mg} \quad (13)$$

The slab thickness parameter has been used to describe patterns of exospheric temperature at planets where the major ionospheric layer occurs within a dominant neutral gas. This occurs for the F2-layer at Earth (Titheridge, 1973), as well as for the M2-layer at Mars (Mendillo et al., 2015).

At Venus, g = 8.87 m/s^2, and using the mass of CO_2 (7.3 × 10^{-26} kg) and Boltzmann's constant (1.38 × 10^{-23} m^2kg/s^2 °K), Eq. (13) can be reconfigured to yield the neutral temperature (°K) from observed values of slab thickness (in km),

$$T_n(^\circ\mathrm{K}) = 11.35 \times \tau(km) \quad (14)$$

This simple relationship allows for insights into Venus' thermosphere (and effectively its exospheric temperature, T_{ex}) over the altitude range where PCE conditions dominate (h ≤ 170 km), and CO_2 remains the dominant neutral gas (confirmed by Figure 5 in Bougher et al., 2015). Thus, the TEC appropriate for use in Eq. (13) is the integral to

170 km, not the full TEC between 100 and 250 km. On average, this PCE-domain value for TEC is typically 76% of the full TEC. As shown in Fig. 9b, the equation for TEC between 100 and 170 km, with a correlation coefficient = 0.98, is:

$$TEC = (1.06 \pm 0.014) \times \sqrt{F_{eff} \times cos(SZA)} - (0.04 \pm 0.115) \left[\text{in units of } 10^{11}\ e^{-}/cm^{2}\right] \quad (15)$$

5.3. Diurnal and solar cycle patterns for temperature of Venus upper atmosphere

Eqs. (11) and (15) provide the climatology for N_mV_2 and TEC as a function of solar flux (F_{eff}) and solar zenith angle (SZA) at Venus' average distance from the Sun. Fig. 10 provides a graphical summary for (a) TEC, (b) N_mV_2, and (c) τ and T_{ex} over the full SZA range for daytime (0 – 90°) conditions, and solar fluxes (F_{eff}) from solar minimum to solar maximum.

There are several aspects to note about Fig. 10. First, the range of values for TEC and N_mV_2 in panels (a) and (b) are large and well correlated, and thus the slab thickness and T_{ex} values shown in panel (c) have a very small numerical range (~12 K for T_{ex})—emphasized by the use of a single color code. For each panel, a vertical slice gives the diurnal variation (SZA = 0° to 90°) for a given solar flux condition (with symmetry assumed for dawn-to- noon and noon-to-dusk). A horizontal slice gives the solar cycle pattern for T_{ex} versus each SZA condition. Examples of these patterns are given in Fig. 11. How do these T_{ex} trends at height ~ 170 km compare with prior observations and models?

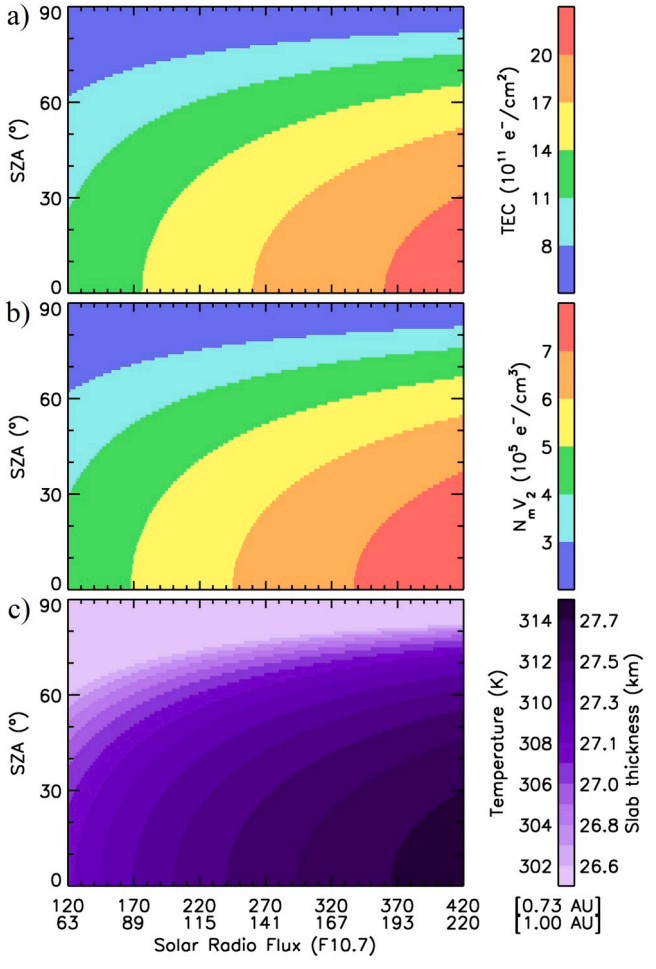

Fig. 10. Summary of the slab thickness (τ) pattern and resultant exospheric temperatures (T_{ex}) derived from the total electron content (TEC) and maximum electron density (N_mV_2) semi-empirical models portrayed by Eqs. (15) and (11), respectively. Panel (a) shows the evaluation of Eq. (15) for TEC over the SZA range of 0°-90° for F_{eff} values at Venus (0.723 AU) from 120 to 420 units (equivalent to 63–220 units at 1 AU); panel (b) shows the evaluation of Eq. (11) for N_mV_2 over the same ranges of SZA and F_{eff}. Panel (c) shows the resultant values of slab thickness (τ = TEC/N_mV_2) and exospheric temperatures (T_{ex}) derived from τ using Eq. (8); note that the same color bar is used for τ in km and T_{ex} in degrees Kelvin.

(a) As summarized in Table 2.6 in Schunk and Nagy (2009), the representative observational value of T_{ex} at Venus is 300 K. The observed diurnal pattern they show in Figure 2.20 (taken from Figure 12 in Niemann et al., 1980) exhibits a broad, and essentially constant, value from post-sunrise to pre-sunset. This is the trend in Fig. 11(a) derived from the slab thickness parameter in Fig. 10. We note, however, that if CO_2 is not the dominant gas in the column content of neutrals up to ~170 km, then the mass (m) value used in Eq. (11) should reflect a mixture of CO_2 and O—leading to lower estimates of exospheric temperatures. Recent modeling results suggesting lower temperatures appear in Gilli et al. (2017) and Gérard et al. (2017).

(b) There are many modeling estimates of diurnal exospheric temperature in the literature, from Dickinson and Bougher (1986) to more recent summaries by Peter et al. (2014), Gérard et al. (2017), Ambili et al. (2019) and Blelly et al. (2019). They all show patterns that support the slab thickness-derived behavior

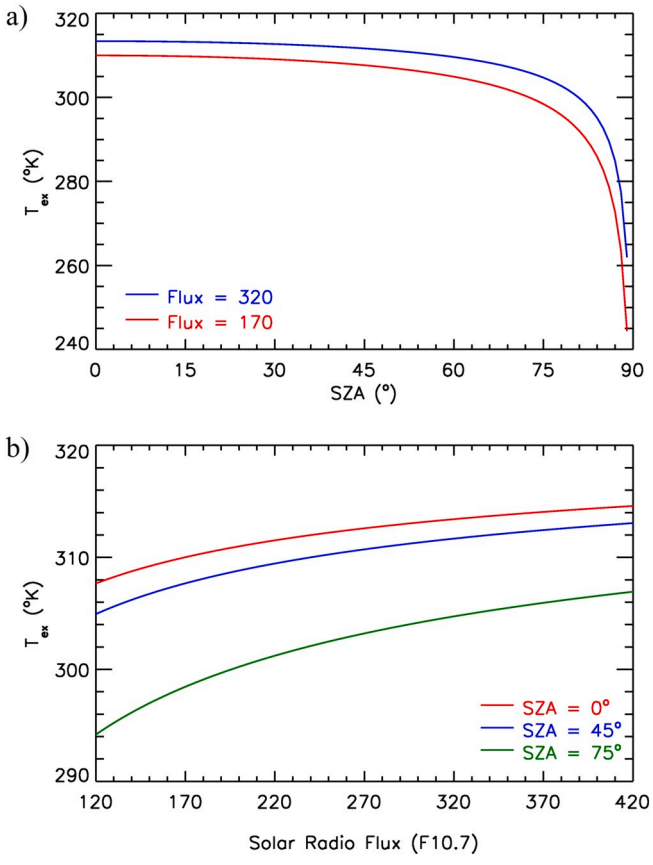

Fig. 11. Examples of exospheric temperatures derived from slab thickness values. Panel (a) shows T_{ex} versus solar zenith angle over the range 0° – 90°. This can be representative of an exospheric pattern depicted as sunrise to noon (right to left) and noon to sunset (left to right). The patterns shown are for solar fluxes (F_{eff}) at 0.723 AU chosen to represent solar minimum and solar maximum conditions. Panel (b) shows T_{ex} versus solar cycle conditions represented by solar fluxes at 0.723 AU for representative solar zenith angles of 0°, 45° and 75°.

suggested here. In Peter et al. (2014), for example, their Fig. 12 shows that the exospheric (asymptotic) temperature begins at ~170 km, and that the VIRA and VenusGRAM models show temperatures essentially constant (275–290 K) throughout the daytime period. Figures 15 and 19 in Gérard et al. (2017) offer additional examples of favorable comparisons.

(c) It is more difficult to find multiple estimates of exospheric temperature versus solar cycle conditions to compare with Fig. 11(b). In the Bougher et al. (1999) Venus model, their Fig. 1 displays profiles of T_{ex} versus height for solar minimum to maximum conditions Their local noon values (230 °K to 310 °K) offer a range of 80 °K, while our pattern in Fig. 11(b) suggests a considerably small range of 10 °K. Yet, from an observational perspective, Forbes et al. (2008) have shown that the thermosphere at Venus responds to long-term changes in solar flux at a rate much lower (~1/5th) than found at Mars. The solar cycle pattern for Venus' exospheric temperature clearly requires more observational and modeling studies.

6. Discussion

The results presented above describe a remarkably stable and consistent ionospheric system under PCE conditions at Venus. The correlations shown in Figs. 3, 6, 8 and 9(b) are essentially perfect. Of course, the altitude region examined was limited to heights where photo-chemical-equilibrium dominates, and thus the planet closest to the Sun might be expected to exhibit the strongest solar control of its ionosphere. Yet, Venus also has a solar-system-unique set of spatial and temporary characteristics relevant to PCE conditions. For example, Venus has the smallest axial tilt (2.7°) among the terrestrial planets, and thus seasonal effects are very small in comparison to those at Earth and Mars (tilts of 23.5° and 25.2°, respectively). Venus also has the most circular orbit of all the planets (eccentricity = 0.007), and thus no orbital influence upon its minimal seasonal variations. Finally, Venus is the planet with by far the slowest rotation period (243 days, retrograde), and thus the "dayside experience" is very long, e.g., a single hour of local (solar) time is equivalent of nearly 5 h of earth time. Taken collectively, Venus exhibits the textbook case of PCE behavior in the solar system.

At Mars, the neutral atmosphere is also dominated by CO_2, and its ionosphere follows the same PCE scheme found at Venus. As described in Mendillo et al. (2017, 2018a), the use of Eq. (8) yielded a correlation coefficient of 0.93 for N_mM_2 and 0.96 for TEC, similar to, but somewhat lower, than found at Venus. For the outer solar system, the application of the PCE Eq. (8) to ionospheric data at Saturn gave very different results. While a background trend with solar activity was found, with a correlation coefficient of 0.50 (Mendillo et al., 2018b), the ionosphere at Saturn is dominated by chemistry associated with influxes of water and other material, and thus not a pure solar-PCE system.

Declaration of competing interest

The authors declare that they have no known competing financial interests or personal relationships that could have appeared to influence the work reported in this paper.

Acknowledgements

Work at Boston University was supported, in part, by the NSF INSPIRE grant #AST-1545581 for studies of comparative ionospheres in the solar system and at exoplanets. MP and ST are funded by the Bundesministerium fuer Wirtschaft, Berlin, via the German Space Agency DLR, Bonn, under grant 50QM1802. KP is funded by the German Research Foundation DFG under grant PA525/14-1.

References

Ambili, K., Babu, S., Choudhary, R., 2019. On the relative roles of the neutral density and photo chemistry on the solar zenith angle variations in the V2 layer characteristics of the Venus ionosphere under different solar activity conditions. Icarus 321, 661–670. https://doi.org/10.1016/j.icarus.2018.12.001.

Bauer, S.J., Lammer, H., 2004. Planetary Aeronomy. Springer, New York.

Blelly, P.-L., et al., 2019. Transplanet: a web service dedicated to modeling of planetary ionospheres. Planet. Space Sci. 169, 35–44. https://doi.org/10.1016/j.pss.2019.02.008.

Bougher, S., et al., 2015. Early MAVEN deep dip campaign reveals thermosphere and ionosphere variability. Science 350, aad0459.

Bougher, S.W., Engel, S., Roble, R.G., Foster, B., 1999. Comparative terrestrial planet thermospheres: 2. Solar cycle variation of global structure and winds at equinox. J. Geophys. Res. 104 (E7), 16591–16611. https://doi.org/10.1029/1998JE001019.

Chapman, S., 1931a. The absorption and dissociative or ionizing effect of monochromatic radiation in an atmosphere on a rotating Earth. Proc. Phys. Soc. 43, 26–45.

Chapman, S., 1931b. The absorption and dissociative or ionizing effect of monochromatic radiation in an atmosphere on a rotating earth, part II, grazing incidence. Proc. Phys. Soc. 43, 483–501.

Colin, L., 1979. Encounter with Venus. Science 203 (4382), 743–745. https://doi.org/10.1126/science.203.4382.743.

Cravens, T.E., Kliore, A.J., Kozyra, J.U., Nagy, A.F., 1981. The ionospheric peak on the Venus dayside. J. Geophys. Res. 86 (A13), 11323–11329. https://doi.org/10.1029/JA086iA13p11323.

Dickinson, R.E., Bougher, S.W., 1986. Venus mesosphere and thermosphere: 1. Heat budget and thermal structure. J. Geophys. Res. 91 (A1), 70–80. https://doi.org/10.1029/JA091iA01p00070.

Forbes, J., Lemoine, F., Bruinsma, S., Smith, M., Zhang, X., 2008. Solar flux variability of Mars' exospheric densities and temperatures. Geophys. Res. Lett. 35, L01201 https://doi.org/10.1029/2007GL031904.

Fox, J., Yeager, K., 2006. Morphology of the near-terminator Martian ionosphere: a comparison of models and data. J. Geophys. Res. 111, A10309 https://doi.org/10.1029/2006JA011697.

Fox, J., Yeager, K., 2009. MGS electron density profiles: analysis of the peak magnitudes. Icarus 200 (2), 468–479. https://doi.org/10.1016/j.icarus.2008.12.002.

Fox, M., Mendillo, M., Klobuchar, J., 1991. Ionospheric equivalent slab thickness and its modeling applications. Radio Sci. 26, 429–438.

Gavrik, A., Gavrik, Y., Withers, P., Joy, S., 2010. Venera 15 and 16 Radio Occultation Ionospheric Electron Density Profile, Version 1.0,V15/V16-V-ROE-5-OCC-ELECTRON-DENS-V1.0. NASA Planetary Data System.

Gérard, J.-C., Bougher, S., Lopez-Valverde, M., Pätzold, M., Drossart, P., Piccioni, G., 2017. Aeronomy of the Venus upper atmosphere. Space Sci. Rev. 212, 1617–1683. https://doi.org/10.1007/s11214-017-0422-0.

Gilli, et al., 2017. Thermal structure of the upper atmosphere of Venus simulated by a ground-to-thermosphere GCM. Icarus 281, 55–72. https://doi.org/10.1016/j.icarus.2016.09.016.

Girazian, Z., Withers, P., 2013. The dependence of peak electron density in the ionosphere of Mars on solar irradiance. Geophys. Res. Lett. 40, 1960–1964. https://doi.org/10.1002/grl.50344.

Girazian, Z., Withers, P., Hausler, B., Patzold, M., Tellmann, S., Peter, K., 2015. Characterization of the lower layer in the dayside Venus ionosphere and comparisons with Mars. Planet. Space Sci. 117, 146–158. https://doi.org/10.1016/j.pss.2015.06.007.

Häusler, B., et al., 2006. Radio science investigations by VeRa onboard the Venus express spacecraft. Planet. Space Sci. 54, 1315–1335. https://doi.org/10.1016/j.pss.2006.04.032.

Kliore, A., Cain, D.L., Levy, G.S., Eshleman, V.R., Fjeldbo, G., Drakem, F.D., 1965. Occultation experiment: results of the first direct measurement of Mars' atmosphere and ionosphere. Science 149, 1243–1248.

Kliore, A., Levy, G.S., Cain, D.L., Fjeldbo, G., Rasool, S.I., 1967. Atmosphere and ionosphere of Venus from the mariner V S-band radio occultation measurement. Science 158, 1683–1688. https://doi.org/10.1126/science.158.3809.1683.

Kliore, A.J., Mullen, L.F., 1989. The long-term behavior of the main peak of the dayside ionosphere of Venus during solar cycle 21 and its implications on the effect of the solar cycle upon the electron temperature in the main peak region. J. Geophys. Res. 94 (A10), 13339–13351. https://doi.org/10.1029/JA094iA10p13339.

Mendillo, M., 2019. The ionospheres of planets and exoplanets. Astronomy & Geophysics 60 (1), 1.25–1.30. https://doi.org/10.1093/astrogeo/atz047.

Mendillo, M., Smith, S., Wroten, J., Rishbeth, H., 2003. Simultaneous ionospheric variability on Earth and Mars. J. Geophys. Res. 108 (A12), 1432. https://doi.org/10.1029/JA00996.

Mendillo, M., Lollo, A., Withers, P., Patzold, M., Tellmann, S., 2011. Modeling Mars' ionosphere with contraints from same-day observations by Mars Global and Mars Express. J. Geophys. Res. 116, A11303. https://doi.org/10.1029/2011JA016865.

Mendillo, M., Marusiak, A., Withers, P., Morgan, D., Gurnett, D., 2013. A new semi-empirical model of the peak electron density of the Martian ionosphere. Geophys. Res. Lett. 40, 5361–5365. https://doi.org/10.1002/2013GL057631.

Mendillo, M., Narvaez, C., Lawler, G., Kofman, W., Mouginot, J., Morgan, D., Gurnett, D., 2015. The equivalent slab thickness of Mars' ionosphere: implications for thermospheric temperature. Geophys. Res. Lett. 42, 3560–3568. https://doi.org/10.1002/2015GL063096.

Mendillo, M., Narvaez, C., Campbell, B., 2017. The total electron content of the Martian ionosphere from MRO/SHARAD observations. J. Geophys. Res.: Planets 122, 182–2192. https://doi.org/10.1002/2017JE005391.

Mendillo, M., et al., 2018a. Mars initial reference ionosphere (MIRI) model: updates and validations using MAVEN, MEX and MRO data sets. J. Geophys. Res. Space Physics 123. https://doi.org/10.1029/2018JA025263.

Mendillo, M., Trovato, J., Moore, L., Muller-Wodarg, I., 2018b. Comparative ionospheres: terrestrial and giant planets. Icarus 303, 34–46. https://doi.org/10.1016/j.icarus.2017.12.033.

Niemann, H., Kasprzak, W., Hedin, A., Hunten, D., Spencer, N., 1980. Mass spectrometric measurements of the neutral gas composition of the thermosphere and exosphere of Venus. J. Geophys. Res. 85 (A13), 7817–7827. https://doi.org/10.1029/JA085iA13p07817.

Pätzold, M., et al., 2007. The structure of Venus' middle atmosphere and ionosphere. Nature 450 (7170), 657–660. https://doi.org/10.1038/nature06239.

Peter, K., et al., 2014. The dayside ionospheres of Mars and Venus: comparing a one-dimensional photochemical model with MaRS (Mars Express) and VeRa (Venus Express) observations. Icarus 233, 66–82. https://doi.org/10.1016/j.icarus.2014.01.028.

Rishbeth, H., Garriott, O.K., 1969. Introduction to Ionospheric Physics. Academic Press, New York.

Rishbeth, H., Mendillo, M., 2004. Ionospheric layers of Mars and Earth. Planetary and Space Science 52 (9), 849–852. https://doi.org/10.1016/j.pss.2004.02.007.

Schunk, R.W., Nagy, A.F., 2009. Ionospheres, 2nd ed. Cambridge Univ. Press, New York. https://doi.org/10.1017/CBO9780511635342.

Smith, F.L., Smith, C., 1972. Numerical evaluation of Chapman's grazing incidence integral ch (X, χ). J. Geophys. Res. 77 (19), 3592–3597. https://doi.org/10.1029/JA077i019p03592.

Titheridge, J.E., 1973. The slab thickness of the mid-latitude ionosphere. Planet. Space Sci. 21, 1775–1793.

Wright, J., 1960. A model of the F region above hmF2. J. Geophys. Res. 65 (1), 185–191.

Zhang, M., Luhmann, J., Kliore, A., 1990. An observational study of the nightside ionosphere of Mars and Venus with radio occultation methods. J. Geophys. Res. 95 (A10), 17,095–17,102.